A LETTERS JOURNAL EXPLORING THE FRONTIERS OF PHYSICS

OFFPRINT

Direct numerical simulation of the axial dipolar dynamo in the Von Kármán Sodium experiment

C. Nore, D. Castanon Quiroz, L. Cappanera and J.-L. Guermond

EPL, **114** (2016) 65002

Please visit the website
www.epljournal.org

Note that the author(s) has the following rights:
– immediately after publication, to use all or part of the article without revision or modification, **including the EPLA-formatted version**, for personal compilations and use only;
– no sooner than 12 months from the date of first publication, to include the accepted manuscript (all or part), **but not the EPLA-formatted version**, on institute repositories or third-party websites provided a link to the online EPL abstract or EPL homepage is included.
For complete copyright details see: https://authors.epletters.net/documents/copyright.pdf.

A Letters Journal Exploring the Frontiers of Physics

AN INVITATION TO SUBMIT YOUR WORK

epljournal.org

The Editorial Board invites you to submit your letters to EPL

EPL is a leading international journal publishing original, innovative Letters in all areas of physics, ranging from condensed matter topics and interdisciplinary research to astrophysics, geophysics, plasma and fusion sciences, including those with application potential.

The high profile of the journal combined with the excellent scientific quality of the articles ensures that EPL is an essential resource for its worldwide audience. EPL offers authors global visibility and a great opportunity to share their work with others across the whole of the physics community.

Run by active scientists, for scientists

EPL is reviewed by scientists for scientists, to serve and support the international scientific community. The Editorial Board is a team of active research scientists with an expert understanding of the needs of both authors and researchers.

OVER
568,000
full text downloads in 2015

18 DAYS
average accept to online publication in 2015

20,300
citations in 2015

"We greatly appreciate the efficient, professional and rapid processing of our paper by your team."

Cong Lin
Shanghai University

Six good reasons to publish with EPL

We want to work with you to gain recognition for your research through worldwide visibility and high citations. As an EPL author, you will benefit from:

1. **Quality** – The 60+ Co-editors, who are experts in their field, oversee the entire peer-review process, from selection of the referees to making all final acceptance decisions.
2. **Convenience** – Easy to access compilations of recent articles in specific narrow fields available on the website.
3. **Speed of processing** – We aim to provide you with a quick and efficient service; the median time from submission to online publication is under 100 days.
4. **High visibility** – Strong promotion and visibility through material available at over 300 events annually, distributed via e-mail, and targeted mailshot newsletters.
5. **International reach** – Over 3200 institutions have access to EPL, enabling your work to be read by your peers in 100 countries.
6. **Open access** – Articles are offered open access for a one-off author payment; green open access on all others with a 12-month embargo.

Details on preparing, submitting and tracking the progress of your manuscript from submission to acceptance are available on the EPL submission website **epletters.net**.

If you would like further information about our author service or EPL in general, please visit **epljournal.org** or e-mail us at **info@epljournal.org**.

EPL is published in partnership with:

European Physical Society | Società Italiana di Fisica | EDP Sciences | IOP Publishing

A Letters Journal Exploring the Frontiers of Physics

June 2016

EPL, **114** (2016) 65002 www.epljournal.org
doi: 10.1209/0295-5075/114/65002

Direct numerical simulation of the axial dipolar dynamo in the Von Kármán Sodium experiment

C. Nore[1], D. Castanon Quiroz[2], L. Cappanera[1,2] and J.-L. Guermond[2]

[1] *Laboratoire d'Informatique pour la Mécanique et les Sciences de l'Ingénieur, LIMSI, CNRS, Univ. Paris-Sud, Université Paris-Saclay - Bât. 508, Campus Universitaire, F-91405 Orsay, France*
[2] *Department of Mathematics, Texas A&M University - 3368 TAMU, College Station, TX 77843-3368, USA*

received 28 March 2016; accepted in final form 15 June 2016
published online 14 July 2016

PACS 52.65.Kj – Magnetohydrodynamic and fluid equation
PACS 47.65.-d – Magnetohydrodynamics and electrohydrodynamics

Abstract – For the first time, a direct numerical simulation of the incompressible, fully nonlinear, magnetohydrodynamic (MHD) equations for the Von Kármán Sodium (VKS) experiment is presented with the two counter-rotating impellers realistically represented. Dynamo thresholds are obtained for various magnetic permeabilities of the impellers and it is observed that the threshold decreases as the magnetic permeability increases. Hydrodynamic results compare well with experimental data in the same range of kinetic Reynolds numbers: at small impeller rotation frequency, the flow is steady; at larger frequency, the fluctuating flow is characterized by small scales and helical vortices localized between the blades. MHD computations show that two distinct magnetic families compete at small kinetic Reynolds number and these two families merge at larger kinetic Reynolds number. In both cases, using ferromagnetic material for the impellers decreases the dynamo threshold and enhances the axisymmetric component of the magnetic field: the resulting dynamo is a mostly axisymmetric axial dipole with an azimuthal component concentrated in the impellers as observed in the VKS experiment.

Copyright © EPLA, 2016

Introduction. – A century or so after it was suggested by Larmor that magnetic fields observed in planets and stars could be generated by dynamo action, the exact mechanism by which a fluid dynamo can be produced in astrophysical bodies is still largely an open problem. This question has resisted experimentation for a long time, and it is only recently that fluid dynamos have been obtained experimentally. There have been only three successful experiments so far: the Riga [1] and the Karlsruhe [2] experiments in 1999, and the Von Kármán Sodium (VKS) experiment [3] in 2006. The observations made in these experiments have been very useful to validate theoretical and numerical dynamo models. For instance, the thresholds for dynamo action in the Riga and the Karlsruhe experiments agreed well with calculations performed with simplified velocity fields and geometries, and the observed magnetic field had the expected spatial distribution. But the results from the VKS experiment were somewhat surprising since dynamo action could be observed only when at least one of the two rotating impellers driving the flow had a high magnetic permeability. Moreover, the magnetic field generated by the device showed a strong axisymmetric component that could not be predicted by simplified axisymmetric velocity fields and geometries. The latest observations in the VKS experiment [4] clearly show that the high magnetic permeability of the impellers is a key factor in the selection of the axisymmetric mode. The exact genesis of the dynamo is not yet fully understood though. The main motivation of the present letter is to present numerical results of the hydrodynamic and magnetohydrodynamic (MHD) regimes in the same geometry as the VKS experiment that produced a magnetic field [3]. These results open the way for further investigations of the dynamo mechanism.

Experimental set-up. – In the following we do direct numerical simulations of the flow driven by the TM73 impellers (for Turbine Métallique, meaning Metal Impeller in French) which were used in the 2006 experiment [3] (see fig. 1). The fluid is liquid sodium heated at 120 °C. The set-up uses two concentric cylindrical containers: one of radius $R_{\rm cyl} = 206\,\text{mm}$ (with a very small thickness) and another thick one, made of copper, of inner and outer

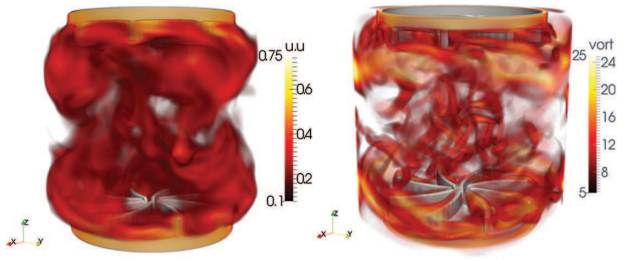

(a) 2 Kinetic energy (b) Vorticity

Fig. 1: (Color online) Navier-Stokes simulations in the TM73 VKS configuration at $R_e = 2500$: (a) full scale for $||\mathbf{u}||_{L^2(\Omega)} = 2\,E(t)$, (b) partial scale for the vorticity field $\boldsymbol{\nabla}\times\mathbf{u}$ (total scale is between 5 and 41).

radius $R_{in} = 289\,\text{mm}$ and $R_{out} = 330\,\text{mm}$, respectively. Both have a total height $H = 412\,\text{mm}$ (we neglect the liquid sodium behind the impellers). The impellers are composed of two disks each supporting 8 blades. The disks have a radius $R_b = 155\,\text{mm}$ and thickness of 20 mm. The blades have an angle of curvature equal to 24°, a height of 41 mm and a thickness of 5 mm. The distance between the inner faces of the disks is set to 370 mm such that the aspect ratio of the fluid is $370/206 = 1.8$ as in the TM73 configuration used in [3] and the TM28 configuration that has been numerically studied in [5] with a penalty method similar to the one used in the present study. The liquid sodium in the inner cylinder is pushed by the convex side of the blades (called the unscooping sense of rotation or (+) sense).

Numerical model. – To investigate the hydrodynamic and MHD regimes of the above experimental set-up, we use our own MHD code called SFEMaNS, which we have been developing, testing and validating since 2002, see [6–10]. This code uses a hybrid spatial discretization mixing Fourier expansions and finite elements. In a nutshell we use a Fourier decomposition in the azimuthal direction such that the problem can be approximated independently (modulo the computations of nonlinear terms) for each Fourier mode in the meridian plane with continuous $\mathbb{P}_1$-$\mathbb{P}_2$ Lagrange elements for the pressure and velocity fields. For the magnetic part, the algorithm solves the problem using the magnetic induction, $\mathbf{b}$, in the conducting region (after standard elimination of the electric field) and the scalar magnetic potential in the insulating exterior. The fields in each region are approximated by using H^1-conforming Lagrange elements, with a technique to enforce $\boldsymbol{\nabla}\cdot\mathbf{b} = 0$ based on a penalty method involving a negative Sobolev norm. This method has been proved to converge under minimal regularity in [10–12] and has been validated in [13], sect. 3.2, and [14–16]. The coupling across the axisymmetric interfaces where the electric conductivity or the magnetic permeability is discontinuous is done by using an interior penalty method. SFEMaNS has been thoroughly validated on numerous manufactured solutions and against other MHD codes (see, *e.g.*, [8,17]).

The reference length L_{ref} is set to R_{cyl}. The domain of computation for the fluid flow is $\Omega = \{(r,\theta,z) \in [0,1]\times[0,2\pi)\times[-1,1]\}$ minus the volume occupied by the moving impellers (disks and blades), henceforth denoted by $\Omega_{imp}(t)$. We refer to [3] for an exact description of the blades. The computational domain for the magnetic field is a larger cylinder composed of the union of Ω, $\Omega_{imp}(t)$ and Ω_{out}, say $\Omega\cup\Omega_{imp}(t)\cup\Omega_{out}$, with $\Omega_{out} = \{(r,\theta,z) \in [1,1.6]\times[0,2\pi)\times[-1,1]\}$. Denoting by σ_0 the electrical conductivity of the liquid sodium, ρ its density, μ_0 the magnetic permeability of vacuum, the magnetic induction is made nondimensional by using $B = U\sqrt{\rho\mu_0}$ (with B and $U = \omega R_{cyl}$ the reference magnetic induction and velocity, respectively, where ω is the angular velocity of the impellers). Two governing parameters appear: $R_m = \mu_0\sigma_0 R_{cyl}^2\omega$ the magnetic Reynolds number and $R_e = R_{cyl}^2\omega/\nu$ the kinetic Reynolds number with ν the kinematic viscosity of the fluid. The nondimensional MHD equations in $\Omega\cup\Omega_{imp}(t)\cup\Omega_{out}$ are

$$\partial_t\mathbf{u} = -(\boldsymbol{\nabla}\times\mathbf{u})\times\mathbf{u} + \frac{1}{R_e}\Delta\mathbf{u} - \boldsymbol{\nabla}p + \mathbf{f}, \tag{1}$$

$$\partial_t\mathbf{b} = \boldsymbol{\nabla}\times(\mathbf{u}\times\mathbf{b}) - \frac{1}{R_m}\boldsymbol{\nabla}\times\left(\frac{1}{\sigma_r}\boldsymbol{\nabla}\times\left(\frac{\mathbf{b}}{\mu_r}\right)\right), \tag{2}$$

$$\boldsymbol{\nabla}\cdot\mathbf{u} = 0, \tag{3}$$

$$\boldsymbol{\nabla}\cdot\mathbf{b} = 0, \tag{4}$$

where $\mathbf{u}$ is the velocity field, $\mathbf{b}$ the induction field (with the magnetic field $\mathbf{h} = \mathbf{b}/\mu_0\mu_r$), p the pressure field, and σ_r, μ_r are the relative conductivity and permeability of the various materials in presence. The parameters σ_r, μ_r are not constant since the walls and the impellers may be composed of copper, steel or soft iron. Specifically we take $\sigma_r = 1$ for $\{(r,\theta,z) \in [1,1.4]\times[0,2\pi)\times[-1,1]\}$ (as for a stagnant lateral layer of liquid sodium) and $\sigma_r = 4.5$ for $\{(r,\theta,z) \in [1.4,1.6]\times[0,2\pi)\times[-1,1]\}$ (as for a lateral copper wall). The Lorentz force $\mathbf{f} = (\boldsymbol{\nabla}\times\mathbf{h})\times\mathbf{b}$ couples the equations. We take $\mathbf{u} = \mathbf{0}$ in Ω_{out}. In the impeller region $\Omega_{imp}(t)$ we take $\mathbf{u} = -\omega r\mathbf{e}_\theta$ in the top impeller and $\mathbf{u} = \omega r\mathbf{e}_\theta$ in the bottom impeller. The no-slip boundary condition is enforced on $\mathbf{u}$ everywhere at the boundary of the fluid domain. In particular, the velocity is forced to be equal to $\pm\omega r$ on the impellers. This is done by using a prediction-correction method of Guermond *et al.* [18] and a pseudo-penalty technique of Pasquetti *et al.* [19]. In summary the Navier-Stokes equations are solved in the fluid region between the blades. The magnetic permeability is $\mu_r = 1$ in $\Omega\cup\Omega_{out}$, *i.e.* in the liquid sodium and in the nonmoving solids. The magnetic permeability in $\Omega_{imp}(t)$ is modeled by a space-dependent function. The local variation of μ_r within the blades is designed to make the permeability maximum inside the blades and equal to 1 at the solid/fluid interface. The maximum reached by the permeability field inside the blades is henceforth denoted by μ_r^{imp}. This method has been thoroughly tested and validated against analytical solutions. Kinematic dynamo results have been

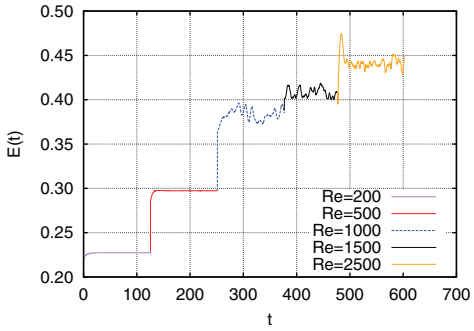

Fig. 2: (Color online) Time evolution of the total kinetic energy at different R_e.

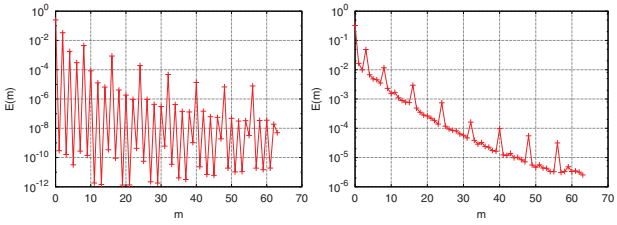

(a) $R_\mathrm{e} = 500$ (b) $R_\mathrm{e} = 2500$

Fig. 3: (Color online) Time-averaged spectra of the kinetic energy as a function of the azimuthal mode.

satisfactorily compared with those computed with a three-dimensional Maxwell code using edge finite elements [15]. Finally we impose perfect ferromagnetic boundary conditions $\mathbf{h}\times\mathbf{n} = \mathbf{0}$ on the outer boundaries of the container to save some computing time. We have compared in [13] the perfect ferromagnetic boundary condition and the vacuum boundary condition in Ohmic decay situations in a geometry similar to that of the VKS setting with flat disks instead of blades (see sect. 4.1, figs. 4, 11(a) and conclusion). Our key conclusion was that the outer boundary conditions: "have only a slight influence on the decay rates [...]. This is surprising, insofar as pseudo vacuum boundary conditions resemble the conditions that correspond to an external material with infinite permeability. Nevertheless, the presence of high-permeability/conductivity disks within the liquid hides the influence of outer boundary conditions [...]". Therefore we are confident that the results presented in the present letter are robust with respect to the boundary condition imposed on the outer shell of the vessel.

Hydrodynamic study. – We first perform hydrodynamic computations by solving eqs. (1) and (3) in the range $R_\mathrm{e} \in [200, 2500]$ with the Lorentz force disabled, *i.e.* $\mathbf{f} = \mathbf{0}$. We will characterize the structure of the flow by representations of the velocity field and by computing various physical quantities as the kinetic energy $E(t) = \frac{1}{2}\|\mathbf{u}\|_{L^2(\Omega)} = \frac{1}{2}\int_\Omega |\mathbf{u}(\mathbf{r},t)|^2 \mathrm{d}\mathbf{r}$. The time average of a quantity f is denoted by $\overline{f}$.

Figure 2 shows the time evolution of the kinetic energy: at $R_\mathrm{e} = 200$ the flow is steady, at $R_\mathrm{e} = 500$ the flow is marginally unsteady, and increasing further R_e leads to a fluctuating regime. Figure 3 shows the time-averaged azimuthal spectra of the kinetic energy: $\overline{E_m} = \overline{\int_{\Omega^{2D}_\mathrm{fluid}} \pi|\hat{\mathbf{u}}(r,m,z,t)|^2 r\mathrm{d}r\mathrm{d}z}$ where $\hat{\mathbf{u}}(r,m,z,t)$ is the m-th Fourier component of the velocity field $\mathbf{u}(r,\theta,z,t)$ and $\Omega^{2D}_\mathrm{fluid}$ is the meridian section of the fluid domain. The maxima at $m = 0$ and $m = 8$ of the energy spectrum correspond respectively to the large scale forcing induced by the rotating disks and to the flow induced by the 8 rotating blades. As expected the steady flow at $R_\mathrm{e} = 200$ is dominated by the $m = 0$ and $m = 8$ modes and their harmonics (data not shown). At $R_\mathrm{e} = 500$ the flow is dominated by the $m = 0$ and $m = 2$ modes: the azimuthal shear layer near the equator acquires a wavy structure with two co-rotating radial vortices as seen in [20]. The spectrum in fig. 3(a) shows that all the even modes are excited by the quadratic nonlinearity of the Navier-Stokes equations. At higher R_e numbers, the $m = 1,2,3$ modes compete with a predominance of the $m = 3$ mode (and still the $m = 0$ and 8 modes) as observed at high Reynolds numbers ($R_\mathrm{e} > 10^5$) in [21]. These modes eventually populate the entire spectrum by nonlinear interactions, and the spectra are more continuous (see fig. 3(b)). Intense helical vortices are generated between the blades as seen in fig. 1 and first numerically evidenced by [5,22].

MHD results. – We now solve the full MHD system, eqs. (1) to (4). The initial velocity field is the velocity obtained at the end of the Navier-Stokes simulations with $R_\mathrm{e} = 500$ or $R_\mathrm{e} = 1500$. The initial magnetic field is a random initial seed. Various MHD runs are performed for different values of the magnetic Reynolds number and relative magnetic permeability of the impellers. Spatial resolution and time steps are reported in table 1. The computations have been done on a parallel machine, but the cumulated amount of computing time used for the simulations presented hereafter is about 5×10^5 hours on one processor.

The onset of dynamo action is monitored by recording the time evolution of the magnetic energy in the conducting domain, $M(t) = \frac{1}{2}\int_{\Omega\cup\Omega_\mathrm{out}} \mathbf{h}(\mathbf{r},t)\cdot\mathbf{b}(\mathbf{r},t)\mathrm{d}\mathbf{r}$, as well as the modal energies $M_m(t) = \int_{\Omega^{2D}\cup\Omega^{2D}_\mathrm{out}} \pi|\hat{\mathbf{h}}(r,m,z,t)|^2 r\mathrm{d}r\mathrm{d}z$. Linear dynamo action occurs when $M_m(t)$ or $M(t)$ is an increasing function of time, and nonlinear dynamo action takes place when the magnetic energies saturate.

We have seen that the flow at $R_\mathrm{e} = 500$ is characterized by the predominance of the even modes for the velocity field. Due to this azimuthal dependence, the eigenvalue problem associated with eqs. (1)–(4) has two disconnected families of magnetic eigenspaces generated by the even and odd Fourier modes. We henceforth refer to these vector spaces as the 0-family and the 1-family, respectively. Given any initial data for eqs. (1)–(4) with nonzero projection on the two families, time integration of the equations

Table 1: Numerical parameters for the MHD computations: kinetic Reynolds number R_e, magnetic Reynolds number R_m, relative magnetic permeability for impellers μ_r^imp, mesh size in the blade region h_min, mesh size at the outer boundary h_max (the meridian mesh is nonuniform), number of Fourier modes, number of processors.

R_e	500	500	500	1500	1500
R_m	$[50, 300]$	–	–	–	–
μ_r^imp	5	50	100	5	50
Δt	2.5×10^{-3}	$1.25{\times}10^{-3}$	–	–	10^{-3}
h_min	2.5×10^{-3}	–	–	–	–
h_max	10^{-2}	–	–	–	–
modes	128	128	160	128	128
nprocs	64	64	160	64	192

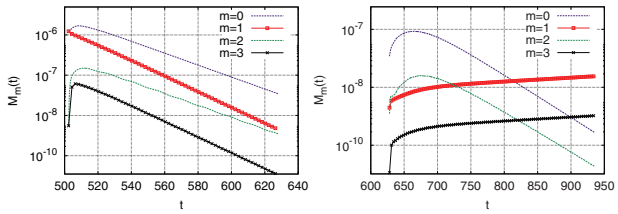

(a) $R_\mathrm{m} = 50$, $\mu_r^\mathrm{imp} = 5$ (b) $R_\mathrm{m} = 150$, $\mu_r^\mathrm{imp} = 5$

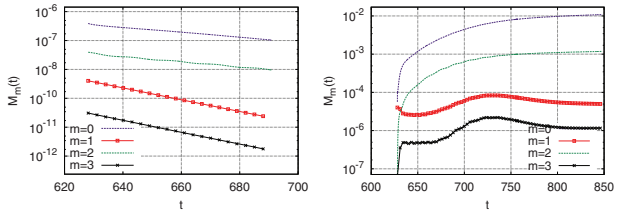

(c) $R_\mathrm{m} = 50$, $\mu_r^\mathrm{imp} = 100$ (d) $R_\mathrm{m} = 150$, $\mu_r^\mathrm{imp} = 100$

Fig. 4: (Color online) Time evolution of the modal magnetic energies $M_m(t)$ for $m = 0, 1, 2, 3$ at $R_\mathrm{e} = 500$ and for $R_\mathrm{m} = 50$ or 150 and $\mu_r^\mathrm{imp} = 5$ or 100 as indicated.

gives a magnetic field which is the superposition of the leading eigenvectors in each family. A typical time evolution of the modal magnetic energy M_m for $m = 0$ to 3 and for $R_\mathrm{m} = 50$ and 150 at $R_\mathrm{e} = 500$ and $\mu_r^\mathrm{imp} = 5$ is shown in fig. 4(a), (b). As expected the two families display two distinct growth rates for each R_m. Note that the 1-family is supercritical before the 0-family at $R_\mathrm{m} = 150$. Linear interpolation of the growth rates determines the critical magnetic Reynolds number R_m^c (*i.e.* when the growth rate is zero), which we have reported in table 2.

Figure 5(a) shows the magnetic field at the final time as reported in fig. 4(b). Note the parallel and anti-parallel vectors near the vertical axis. We observe the expected $m = 1$ eigenmode evidenced in kinematic dynamo computations in [17] (see fig. 2(d) therein). This mode is characterized by an equatorial dipole with two opposite axial structures mainly localized in the bulk of the fluid.

Table 2: Magnetic thresholds for $R_\mathrm{e} = 500$: 0-f and 1-f indicate the 0-family and 1-family, respectively.

μ_r	R_m^c(0-f)	R_m^c(1-f)	P_m^c(0-f)	P_m^c(1-f)
5	240 ± 5	147 ± 1	≈ 0.48	≈ 0.29
50	130 ± 2	138 ± 2	≈ 0.26	≈ 0.28
100	82 ± 2	144 ± 2	≈ 0.16	≈ 0.29

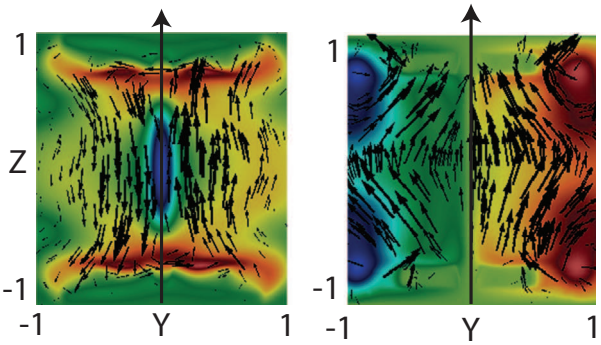

(a) $\mu_r^\mathrm{imp} = 5$ (b) $\mu_r^\mathrm{imp} = 100$

Fig. 5: (Color online) Magnetic field from full MHD simulations in the TM73 VKS configuration at $R_\mathrm{e} = 500$, $R_\mathrm{m} = 150$ and (a) $\mu_r^\mathrm{imp} = 5$ (1-family) at the final time of fig. 4(b), (b) $\mu_r^\mathrm{imp} = 100$ (0-family) at the final time of fig. 4(d). Arrows represent in-plane $\{h_y, h_z\}$ vectors and color represents the out-of-plane component h_x (from blue to red: $-2\times10^{-4} \le h_x \le 2.5\times10^{-4}$, $-1.4 \times 10^{-1} \le h_x \le 1.4 \times 10^{-1}$, respectively). The cylinder axis is indicated by a vertical arrow. Only the fluid domain Ω is represented.

Observing this structure at small R_e is compatible with the kinematic dynamo results previously published. Note that the critical magnetic Prandtl number P_m^c for the 1-family mode does not vary significantly with respect to μ_r^imp and it is always smaller than 1.

An estimate of the effective magnetic permeability of the soft iron TM73 impellers used in [3] is $\mu_r^\mathrm{imp} \approx 65$ [23]. Therefore we vary the relative permeability of the impellers. Increasing μ_r^imp enhances the 0-family growth rates (see fig. 4(c), (d)) and switches the ordering of the thresholds. Note that the 1-family thresholds barely change with μ_r^imp, because the corresponding eigenmode is localized mainly in the bulk, while the 0-family thresholds vary dramatically, because the corresponding eigenmode is characterized by an azimuthal magnetic component concentrated in the impellers and an axial dipole in the bulk (see fig. 5(b) showing the saturated state).

At $R_\mathrm{e} = 1500$ the flow is more fluctuating and all the velocity modes are coupled with a predominance of the $m = 0$ and $m = 3$ modes. Therefore there is no distinct magnetic family and the eigenmode is mainly axisymmetric. Computations need more spatial resolution and CPU time (see table 1). We have tested two relative permeabilities $\mu_r^\mathrm{imp} \in \{5, 50\}$ and found that the threshold decreases with μ_r^imp (see table 3). The modal

Table 3: Magnetic thresholds for $R_e = 1500$.

μ_r	R_m^c	P_m^c
5	130 ± 5	≈ 0.09
50	90 ± 5	≈ 0.06

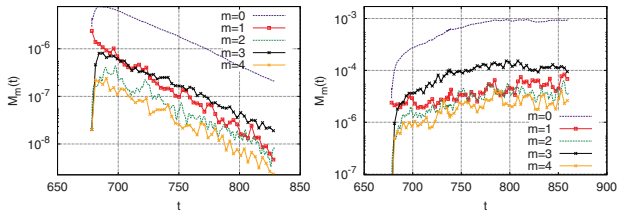

(a) $R_m = 50$ (b) $R_m = 100$

Fig. 6: (Color online) Time evolution of the modal magnetic energies $M_m(t)$ for $m \in [0, 4]$ and for $R_m = 50$ and 100 at $R_e = 1500$ and $\mu_r^{imp} = 50$.

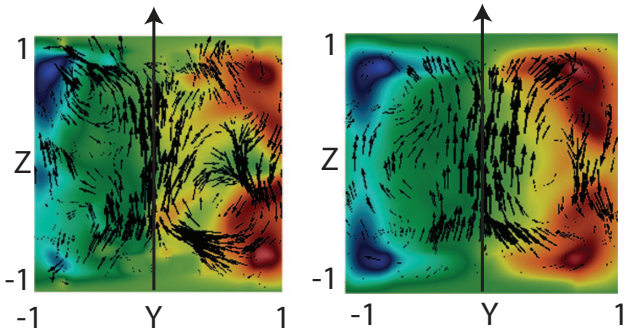

(a) Instantaneous magnetic field (b) Time-averaged magnetic field

Fig. 7: (Color online) Magnetic field from full MHD simulations in the TM73 VKS configuration in the saturated regime at $R_e = 1500$, $R_m = 150$ and $\mu_r^{imp} = 50$. Arrows represent in-plane $\{h_y, h_z\}$ vectors and color represents the out-of-plane component h_x (from blue to red: $-5.3 \times 10^{-2} \leq h_x \leq 5.4 \times 10^{-2}$, $-2.8 \times 10^{-2} \leq h_x \leq 3.1 \times 10^{-2}$, respectively). The cylinder axis is indicated by a vertical arrow. Only the fluid domain Ω is represented.

magnetic energies for the $m \in [0, 4]$ modes show that the $m = 0$ and $m = 3$ magnetic modes are coupled as well as $m = 1$ and $m = 4$ modes because of the predominance of the $m = 3$ mode in the velocity field (see fig. 6) and through the coupling via the electromotive term $\mathbf{u} \times \mathbf{b}$. An illustrative view of the mainly axisymmetric magnetic field generated at saturation is displayed in fig. 7. The radial component is odd with respect to z, whereas the azimuthal and vertical components are even and of opposite sign. These features are compatible with the magnetic field measured at saturation in the experimental dynamo regime obtained with two counter-rotating soft iron impellers (see fig. 6(b) in [24]). Using a ferromagnetic material decreases the dynamo threshold and enhances the predominantly axisymmetric magnetic field.

Discussion and perspectives. – Our results show for the first time that the ferromagnetic impellers are crucial to obtain the predominantly axisymmetric dynamo mode in a VKS configuration in a full-MHD model at moderate kinetic Reynolds numbers. Increasing R_e from 500 to 1500 decreases the dynamo threshold and a numerical challenge would be to extend the range of R_e in numerical simulations. Different dynamo mechanisms have been proposed or tested in this VKS set-up: an α-Ω dynamo loop in [14,16,25,26], α^2 or α^2-Ω cycles in [22]. A future study aiming at exploring the saturation regime and measuring the helicity tensor is currently engaged to discriminate between these various scenarios. However extraction of transport coefficients from DNS results is a highly non-trivial undertaking (see, *e.g.*, [27,28]).

* * *

The HPC resources were provided by GENCI-IDRIS (grant 2015-0254) in France and by the Texas A&M University Brazos HPC cluster. J-LG acknowledges support from Univ. Paris Sud, the National Science Foundation, under grants NSF DMS-1015984, DMS-1217262, the Air Force Office of Scientific Research, USAF, under grant/contract No. FA9550-15-1-0257, and the Army Research Office under grant/contract No. W911NF-15-1-0517.

REFERENCES

[1] Gailitis A. *et al.*, *Phys. Rev. Lett.*, **84** (2000) 4365.
[2] Stieglitz R. and Müller U., *Phys. Fluids*, **13** (2001) 561.
[3] Monchaux R. *et al.*, *Phys. Rev. Lett.*, **98** (2007) 044502.
[4] Miralles S. *et al.*, *Phys. Rev. E*, **88** (2013) 013002.
[5] Kreuzahler S. *et al.*, *New J. Phys.*, **16** (2014) 103001.
[6] Guermond J. L., Léorat J. and Nore C., *Eur. J. Mech. B/Fluids*, **22** (2003) 555.
[7] Guermond J.-L., Laguerre R., Léorat J. and Nore C., *J. Comput. Phys.*, **221** (2007) 349.
[8] Guermond J.-L., Laguerre R., Léorat J. and Nore C., *J. Comput. Phys.*, **228** (2009) 2739.
[9] Guermond J.-L., Léorat J., Luddens F., Nore C. and Ribeiro A., *J. Comput. Phys.*, **230** (2011) 6299.
[10] Bonito A., Guermond J.-L. and Luddens F., *J. Math. Anal. Appl.*, **408** (2013) 498.
[11] Bonito A., Guermond J.-L. and Luddens F., to be published in *ESAIM/M2AN Math. Model. Numer. Anal.*, `http://dx.doi.org/10.1051/m2an/2015086` (2016).
[12] Bonito A. and Guermond J.-L., *Math. Comput.*, **80** (2011) 1887.
[13] Giesecke A. *et al.*, *Geophys. Astrophys. Fluid Dyn.*, **104** (2010) 505.
[14] Giesecke A., Stefani F. and Gerbeth G., *Phys. Rev. Lett.*, **104** (2010) 044503.
[15] Nore C., Zaidi H., Bouillault F., Bossavit A. and Guermond J.-L., *COMPEL*, **35** (2016) 326.
[16] Nore C., Léorat J., Guermond J.-L. and Giesecke A., *Phys. Rev. E*, **91** (2015) 013008.

[17] Giesecke A. *et al.*, *New J. Phys.*, **14** (2012) 053005.
[18] Guermond J.-L. and Shen J., *Math. Comput.*, **73** (2004) 1719.
[19] Pasquetti R., Bwemba R. and Cousin L., *Appl. Numer. Math.*, **58** (2008) 946.
[20] Ravelet F., Chiffaudel A. and Daviaud F., *J. Fluid Mech.*, **601** (2008) 339.
[21] Cortet P.-P. *et al.*, *Phys. Fluids*, **21** (2009) 025104.
[22] Ravelet F., Dubrulle B., Daviaud F. and Ratié P.-A., *Phys. Rev. Lett.*, **109** (2012) 024503.
[23] Verhille G. *et al.*, *New J. Phys.*, **12** (2010) 033006.
[24] Boisson J. *et al.*, *New J. Phys.*, **14** (2012) 013044.
[25] Pétrélis F., Mordant N., and Fauve S., *Geophys. Astrophys. Fluid Dyn.*, **101** (2007) 289.
[26] Laguerre R. *et al.*, *Phys. Rev. Lett.*, **101** (2008) 104501.
[27] Rheinhardt M. and Brandenburg A., *Astron. Astrophys.*, **520** (2010) A28.
[28] Schrinner M., Rädler K.-H., Schmitt D., Rheinhardt M. and Christensen U., *Geophys. Astrophys. Fluid Dyn.*, **101** (2007) 81.